

Scalable high-fidelity and near-deterministic preparation of large photon-number states

Mo Xiong,^{1,*} Jize Han,^{2,1,*} Chuanzhen Cao,¹ Jinbin Li,^{1,3} Zhiguo Huang,² and Ming Xue^{1,3,†}

¹College of Physics, Nanjing University of Aeronautics and Astronautics, Nanjing 211106, China

²China Mobile (Suzhou) Software Technology Co., Ltd., Suzhou, 215163, China

³Key Laboratory of Aerospace Information Sensing and Physics (NUAA), MIIT, Nanjing 211106, China

(Dated: March 31, 2026)

The scalable preparation of large photon-number (Fock) states is a long-standing frontier in quantum science, with direct implications for quantum metrology and bosonic quantum information processing. Despite substantial progress at small photon numbers, extending state generation to large photon numbers while maintaining high fidelity and operating deterministically remains a significant challenge. Here we demonstrate a scalable and experimentally accessible control protocol for generating large photon-number states using only native spin-oscillator operations. The protocol alternates Jaynes–Cummings interactions with phase-space displacements to imprint photon-number-dependent phases and convert them into selective interference in photon-number space. It already achieves high preparation fidelity unconditionally, while an optional final qubit projection removes residual qubit–field correlations and further enhances the fidelity. Conditioned on this final projection, photon-number state preparation with fidelities exceeding 0.95 is achieved for photon numbers in the few-hundred regime, with a success probability exceeding 0.90, placing the protocol in a near-deterministic operating regime. The resulting control sequences remain shallow and are robust against detuning, control noise, and experimentally relevant dissipation. Our results establish a practical route to scalable, high-fidelity photon-number state preparation at large photon numbers and provide a versatile interference-engineering toolbox for nonclassical bosonic state synthesis.

I. INTRODUCTION

The ability to deterministically prepare highly nonclassical bosonic states is a central goal in quantum science, with far-reaching implications for quantum metrology, communication, simulation, and fault-tolerant quantum technologies [1–11]. Among these states, photon-number (Fock) states $|N\rangle$ —energy eigenstates with a precisely defined number of excitations—constitute fundamental non-Gaussian resources [12–14]. As the excitation number increases, large- N photon-number states exhibit increasingly fine phase-space interference and enhanced sensitivity to external perturbations, thereby enabling superior performance in precision sensing [15–17] and bosonic quantum information protocols [18, 19]. At the same time, these very properties render their scalable and deterministic preparation particularly challenging.

Over the past decades, remarkable progress has been achieved in generating single- and few-excitation photon-number states across a wide range of experimental platforms [20–27]. However, extending such capabilities to large photon numbers remains elusive [28–39]. Most existing approaches rely on probabilistic processes, including measurement-based filtering [16, 40, 41], or exploit bosonic nonlinearities [42–46], or dissipation engineering [47]. Deterministic schemes based on sequential population transfer or photon-number subtraction or addition [22, 35, 48–50], on the other hand, require an increasing number of elementary operations as N grows, leading to rapid accumulation of control errors and decoherence. Despite their effectiveness at small scales, all these

approaches are ultimately constrained by fundamental trade-offs between determinism, robustness, and scalability.

From a broader control perspective, these difficulties reflect an inherent trade-off between available control resources and the complexity of the required control protocols, which becomes increasingly restrictive as the target photon-number grows. These challenges point to a more general obstacle: the difficulty of engineering strong and well-controlled photon-number-dependent phases across a large bosonic Hilbert space [51–55]. Despite important advances, achieving deterministic, scalable, and high-fidelity preparation of large- N photon-number states remains an open problem, and continued exploration of diverse and complementary approaches is both necessary and valuable.

Here we formulate large photon-number state preparation as a task of engineering interference through time-structured, photon-number-dependent dynamics, rather than relying on sequential population transfer or bosonic nonlinearities. This perspective reframes the problem from population engineering to coherent interference engineering in Fock space. Our approach exploits the intrinsic nonlinear spectrum of the Jaynes–Cummings (JC) interaction, which naturally generates photon-number-dependent phase accumulation while remaining natively available across a wide range of experimental platforms, including cavity and circuit quantum electrodynamics (QED) [56, 57], trapped ions [58, 59], and other atomic, molecular, and optical (AMO) systems [60]. By combining JC interactions with phase-space displacement operations, we construct composite control sequences that deterministically reshape an initial coherent-state distribution through engineered interference in photon-number space.

We demonstrate the generation of large photon-number states with fidelities exceeding 0.95 up to $N \simeq 200$, with success probabilities above 0.90 upon optional post-selection. The resulting protocols employ only native spin-oscillator op-

* These authors contributed equally to this work.

† Corresponding author: mxue@nuaa.edu.cn

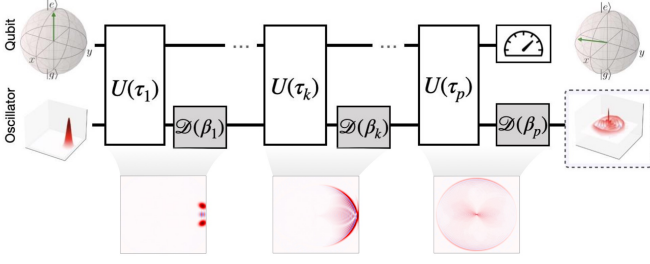


Figure 1. **Multi-pulse JC-displacement protocol for Fock-state generation.** The control sequence consists of p layers, each comprising a resonant JC evolution $U(\tau_k)$ acting on the joint qubit-oscillator system, followed by a phase-space displacement $D(\beta_k)$ applied to the bosonic mode. The qubit is initialized in the excited state and the oscillator in a coherent state. Repeated accumulation of photon-number-dependent phases arising from the nonlinear JC spectrum, combined with displacement-induced interference, progressively reshapes the oscillator state in phase space. The second row shows representative Wigner-function snapshots at different layers of the protocol, illustrating the emergence of nonclassical interference fringes characteristic of large photon-number states. A final projective measurement on the qubit can be used to disentangle the qubit from the oscillator.

erations, require shallow control depths, and exhibit robustness against detuning, control noise, and dissipation. Our results establish a scalable and experimentally accessible route toward high-fidelity photon-number state generation, opening new opportunities for quantum-enhanced sensing and bosonic quantum technologies.

II. MODEL AND PROTOCOL

A. Composite-pulse protocol

We consider a spin-boson interaction in which a two-level system couples to a single-mode quantized field. This standard setting, as described by the JC Hamiltonian, captures the essential physics of light-matter interaction across cavity QED, circuit QED, and related platforms. In the rotating frame ($\hbar = 1$), the Hamiltonian reads

$$\hat{H} = -\Delta \hat{a}^\dagger \hat{a} + \Omega(\hat{a} \hat{\sigma}_+ + \hat{a}^\dagger \hat{\sigma}_-), \quad (1)$$

where $\Delta = \omega_q - \omega_c$ denotes the detuning between the qubit and cavity frequencies ($\Delta = 0$ hereafter for the resonant case), and Ω is the coupling strength. The operators \hat{a} (\hat{a}^\dagger) annihilate (create) photons in the cavity mode, while $\hat{\sigma}_-$ ($\hat{\sigma}_+$) = $|g\rangle\langle e|$ ($|e\rangle\langle g|$) lower (raise) the qubit between its ground and excited states $|g\rangle$ and $|e\rangle$.

Our objective is to prepare a target Fock state $\rho_N = |N\rangle\langle N|$ of the bosonic mode. The protocol begins with the cavity initialized in a coherent state $|\alpha\rangle$ of mean photon-number $|\alpha|^2 = N$, which provides a physically natural and experimentally accessible seed for photon-number state synthesis. The full initial state is therefore $|\Psi_0\rangle = |e\rangle|\alpha\rangle$.

As depicted in Fig. 1, the control sequence consists of p composite pulses alternating between JC evolution and

phase-space displacement operations. The sequence is fully specified by $\{\tau, \beta\}$, where $\tau = (\tau_1, \dots, \tau_p)$ and $\beta = (\beta_1, \dots, \beta_p)$. After the full sequence, the joint atom-field state is

$$|\Psi(\tau, \beta)\rangle = \left[\prod_{k=1}^p \hat{D}(\beta_k) \hat{U}(\tau_k) \right] |\Psi_0\rangle, \quad (2)$$

where $\hat{U}(\tau_k) = e^{-i\hat{H}\tau_k}$ is JC evolution of duration $\tau_k \in \mathbb{R}^+$, and $\hat{D}(\beta_k) = e^{\beta_k \hat{a}^\dagger - \beta_k^* \hat{a}}$ displaces the field by amplitude $\beta_k \in \mathbb{C}$.

A key structural feature of the protocol is the time-control index (ℓ), which specifies the total evolution time through its relation to the JC quantum revival structure [61, 62]:

$$\Omega T_R^{(\ell)} \approx (2\ell + 1)\pi\sqrt{N}. \quad (3)$$

For a single-layer circuit ($p = 1$), choosing $\ell = 1$ reproduces the revival-time operation of Ref. [38]. In the multi-pulse setting, however, the interplay between multiple JC segments and displacement operations generates a much richer interference landscape. Accordingly, the control parameters are defined under the global timing scale set by $T_R^{(\ell)}$, while leaving the internal pulse structure unconstrained.

The cavity state resulting from this sequence may be obtained directly by tracing the qubit, or, alternatively, via a projective measurement on the qubit (cf. Fig. 1). In the latter case, the qubit is projected onto $|\psi_q\rangle = \cos(\varphi_0/2)|g\rangle + \sin(\varphi_0/2)e^{i\varphi_1}|e\rangle$ with $\varphi = \{\varphi_0, \varphi_1\}$, which removes the remaining atom-field correlations and yields a purer cavity state. This optional post-selection step removes the residual qubit-field correlations and yields a purer cavity state, with a success probability close to unity.

High-fidelity preparation is obtained by optimizing over the $3p + 2$ control parameters

$$\theta = \{\tau, \beta, \varphi\}, \quad (4)$$

where $\tau = (\tau_1, \dots, \tau_p)$ and $\beta = (\beta_1, \dots, \beta_p)$ specify the durations and complex displacements of the p composite layers, and $\varphi = \{\varphi_0, \varphi_1\}$ defines the (optional) qubit projection basis. The quality of the prepared cavity state ρ_θ is quantified by its Uhlmann-Jozsa fidelity with the target Fock state $\rho_N = |N\rangle\langle N|$,

$$\mathcal{F}(\theta) = \left(\text{Tr} \sqrt{\sqrt{\rho_\theta} \rho_N \sqrt{\rho_\theta}} \right)^2. \quad (5)$$

To avoid repeated reduced-state evaluations during the search, we instead minimize the proxy loss

$$\mathcal{L}_\theta = 1 - |\langle \Psi(\tau, \beta) | \Psi_N(\varphi) \rangle|^2, \quad (6)$$

where $|\Psi_N(\varphi)\rangle = |\psi_q(\varphi)\rangle \otimes |N\rangle$ denotes the ideal disentangled target state. This variational formulation naturally generalizes the single-pulse JC approach to a richer multi-pulse control landscape and enables efficient numerical optimization of composite sequences.

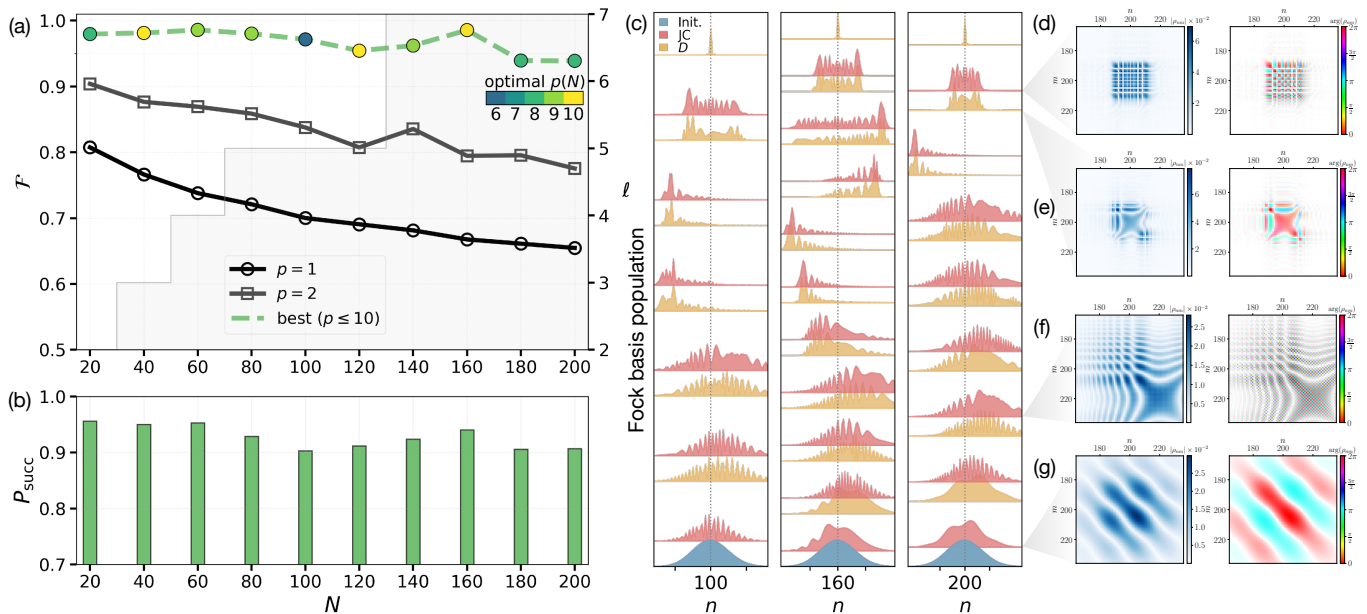


Figure 2. Multi-pulse JC-displacement protocol for large- N photon-number state generation. (a) Target-Fock fidelity \mathcal{F} as a function of photon-number N for $p = 1$, $p = 2$, and the optimized multi-pulse protocol ($p \leq 10$). Colored markers indicate the optimal pulse number $p(N)$ for each N . The grey staircase in the background shows the corresponding optimal interaction index ℓ . (b) Post-selection success probability P_{succ} for the optimized protocol, demonstrating that high fidelity is achieved without sacrificing projection efficiency. (c) Waterfall plots of the photon-number basis populations during the sequential JC interaction and displacement operations (bottom to top) for representative $N = 100, 160, 200$. Each layer shows the population immediately after a JC step (red) and after the subsequent displacement \hat{D} (gold), with the initial Poisson distribution shown in blue. The protocol progressively reshapes the broad coherent-state distribution into a sharply localized photon-number component (vertical dashed line marks the target $n = N$). (d)–(g) Density-matrix snapshots illustrating the evolution of magnitude $|\rho_{nm}|$ (left) and phase $\arg(\rho_{nm})$ (right). The multi-pulse sequence first imprints nonlinear number-dependent phases via JC dynamics and subsequently converts them into constructive interference through displacement, resulting in coherent focusing along the target photon-number diagonal. The final state exhibits a dominant diagonal element with suppressed off-diagonal weight, consistent with high-fidelity photon-number state preparation.

In practice, the non-convex landscape associated with Eq. (6) contains many periodic local minima. Throughout this work, the parameters θ are obtained using a hybrid genetic–Adam (GAdam) optimization routine. To accelerate the search and enforce a physically meaningful global timing scale, the depth- p optimization is typically seeded via transfer initialization from an optimized single-layer ($p = 1$) solution at the same (N, ℓ) , which provides an effective starting point for the subsequent multi-pulse refinement (see Methods for detail).

B. Fidelity and dynamics

Fig. 2 benchmarks our protocol and highlights its encouraging scaling with photon-number N . As seen in Fig. 2(a), increasing the depth from the single-layer baseline ($p = 1$) to $p = 2$ already mitigates the fidelity loss with N , while the optimized protocol (best, $p \leq 10$) exhibits only weak degradation over the explored range. The optimized sequences achieve post-selected fidelities $\mathcal{F} \geq 0.95$ for all targets up to $N = 160$, and remain only slightly below 0.95 at $N = 180, 200$. The optimal depth $p(N)$ (colored markers) grows slowly with N , while the interaction-time index ℓ (grey

staircase) sets a global timing scale. High fidelity is retained in a near-deterministic regime, with $P_{\text{succ}} \gtrsim 0.90$ throughout [Fig. 2(b)], indicating that the final projection primarily purifies the cavity state by removing residual qubit–field correlations. The mild degradation at the largest N is obtained under a fixed optimization budget and is therefore conservative.

The dynamical reshaping is visualized in the waterfall plots of Fig. 2(c) for representative $N = 100, 160, 200$. Starting from the broad Poissonian seed (blue) and proceeding from bottom to top along the pulse sequence, each JC segment (red) introduces pronounced oscillatory structure while redistributing population only locally within the existing photon-number support. The subsequent displacement (gold) then produces the dominant envelope reshaping and a systematic concentration toward $n = N$, culminating in a sharply localized final peak.

Each JC segment reshuffles populations only locally in the Fock basis and transfers weight only between adjacent photon-number states and hence preserves a broad envelope at early stages. The dominant role of the JC segment is instead to imprint a nonlinear, number-dependent phase structure onto photon-number space coherences.

The phase snapshots $\arg(\rho_{nm})$ in Figs. 2(d)–(g) provide a direct signature of the nonlinear JC spectrum (right

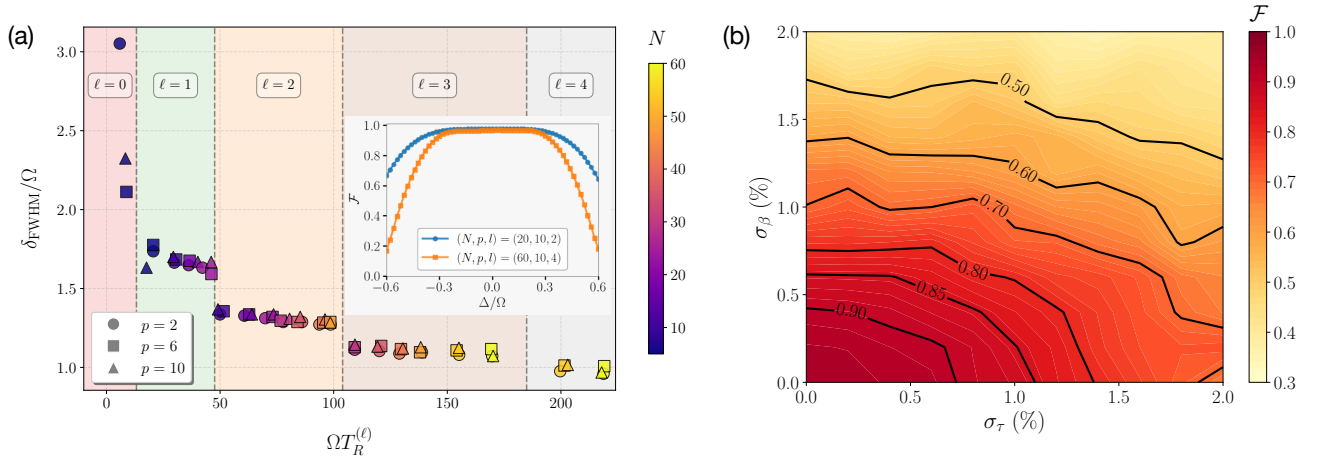


Figure 3. **Robustness of the multi-pulse protocol against detuning, control noise.** (a) Detuning tolerance quantified by the full width at half maximum (FWHM) of $\bar{\mathcal{F}}(\Delta/\Omega)$ as a function of the protocol time scale $\Omega T_R^{(\ell)}$ for different ℓ -families. Marker shapes denote the circuit depth p and colors indicate the target photon-number N . Inset: representative linecuts of $\mathcal{F}(\Delta/\Omega)$ at $p = 10$. (b) Average post-selected fidelity $\bar{\mathcal{F}}$ under timing and displacement errors for $N = 100$ ($p = 10, \ell = 4$), averaged over 200 realizations of independent Gaussian perturbations with standard deviations σ_τ and σ_β .

panels). Because the resonant dressed splittings $E_{n,\pm} = \pm\Omega\sqrt{n+1}$ vary nonlinearly with photon-number, different photon-number components accumulate different phases. In the semiclassical pointer-state picture [61], this nonlinearity can be made explicit by expanding \sqrt{n} for n in the vicinity of a large target photon-number N ,

$$\sqrt{n} = \sqrt{N} + \frac{\delta n}{2\sqrt{N}} - \frac{\delta n^2}{8N^{3/2}} + \dots, \quad \delta n \equiv n - N, \quad (7)$$

which separates a leading linear phase gradient from a shear-like quadratic contribution. This number dependence first appears as clear band-like phase structures [Fig. 2(g)], and then evolves into visibly curved bands as higher-order contributions become important [Figs. 2(f) and 2(e)]. In later layers, repeated alternation of JC evolution (nonlinear phase accumulation) and displacement (phase-sensitive mixing) progressively organizes the phase texture, approaching an anti-diagonal alignment of the mirror-symmetric coherence ridge near $n + m \simeq 2N$ immediately before the final displacement step, thereby preparing the interference condition for the final focusing.

C. Robustness analysis

We evaluate the robustness of the protocol against experimentally relevant imperfections, grouped into (i) systematic control errors, including qubit–oscillator detuning and inaccuracies in pulse timing and displacement amplitude; and (ii) environment-induced errors from open-system dynamics such as cavity photon loss and qubit spontaneous emission.

Detuning robustness. We first consider qubit–oscillator detuning $\Delta = \omega_q - \omega_c$. The dependence of the post-selected fidelity on detuning is illustrated in the inset of Fig. 3(a) for a representative circuit depth $p = 10$. For small photon num-

bers ($N = 20$), the fidelity remains close to unity over a broad range of Δ/Ω , whereas for larger photon numbers ($N = 60$) the high-fidelity plateau becomes noticeably narrower, reflecting the increased sensitivity of high- N photon-number states to detuning-induced phase accumulation during the JC evolution. This behavior is quantified in Fig. 3(a), where the detuning tolerance is characterized by the full width at half maximum δ_{FWHM} as a function of the total evolution time $\Omega T_R^{(\ell)}$ for different circuit depths p . For small photon numbers or short total evolution times, δ_{FWHM} shows a clear dependence on the number of control layers: increasing p introduces additional phase structure and control complexity, which can reduce the effective detuning bandwidth. In contrast, for larger photon numbers the data for $p = 2, 6$, and 10 collapse onto a common trend and the extracted δ_{FWHM} tends to saturate, indicating a time-limited regime in which detuning-induced phase errors are governed primarily by the total accumulated interaction time rather than by the specific segmentation of the sequence; this saturation is favorable for high- N operation since the detuning bandwidth does not continue to shrink rapidly as N increases.

Pulse errors. We next analyze the impact of control inaccuracies in the JC evolution times and displacement amplitudes. The implemented control parameters are modeled as

$$\tau_k = \tau_k^* + \xi_k^\tau, \quad \beta_k = \beta_k^* + \xi_k^\beta, \quad (8)$$

where the noise variables ξ_k^τ and the real and imaginary parts of ξ_k^β are sampled independently from zero-mean Gaussian distributions with variances σ_τ^2 and σ_β^2 , respectively.

Fig. 3(b) shows the resulting fidelity landscape for the $N = 100$ target with $p = 10$ and $\ell = 4$, where each point corresponds to the post-selected fidelity $\bar{\mathcal{F}}$ averaged over 200 independent realizations of the control errors. A broad high-fidelity basin persists around the optimum. In particular, sub-percent timing errors and displacement miscalibrations pre-

serve a near-ideal performance: for $(\sigma_\tau, \sigma_\beta) \lesssim (0.5\%, 0.5\%)$, we find $\mathcal{F} \gtrsim 0.90$ for the $N = 100$ target. For qubit–oscillator coupling strengths in the range $\Omega/2\pi \sim \text{kHz–MHz}$, typical of current cavity or circuit QED platforms, the total evolution time T_N spans from several tens of milliseconds down to the sub-millisecond regime. Each JC segment therefore has a characteristic duration $\tau_k \sim T_N/p$, placing it in the sub-millisecond to millisecond range across these platforms. In practical AMO experiments [60], the evolution time of a gate operation is typically controlled by an arbitrary waveform generator with sampling rates reaching the gigahertz regime, enabling temporal accuracy at the level of a few tens of nanoseconds. Comparing these timescales indicates that relative timing errors can be well controlled below the percent level under realistic experimental conditions [63]. The displacement amplitudes can be calibrated with reliable experimental control and stability [11, 16, 52, 64].

Dissipation effects. We finally evaluate the performance of the multi-pulse protocol in the presence of open-system dynamics arising from cavity photon loss and atomic spontaneous emission. The system evolution is modeled by the Lindblad master equation $\dot{\rho}(t) = -i[\hat{H}, \rho(t)] + \frac{\kappa}{2}\mathcal{D}[\hat{a}]\rho + \frac{\Gamma}{2}\mathcal{D}[\hat{\sigma}_-]\rho$, where κ and Γ denote the cavity decay and atomic spontaneous emission rates, respectively, and $\mathcal{D}[\hat{o}]\rho = 2\hat{o}\rho\hat{o}^\dagger - \hat{o}^\dagger\hat{o}\rho - \rho\hat{o}^\dagger\hat{o}$ is the Lindblad superoperator. A convenient dimensionless figure of merit that summarizes the competition between coherent JC dynamics and dissipation is the single-atom cooperativity $C \equiv \Omega^2/\kappa\Gamma$.

A particularly promising direction is provided by atom-array cavity QED, where two-dimensional ordered atomic arrays in free space form an effective optical cavity with well-defined cavity-QED parameters. Recent cavity-array experiments and near-term proposals already operate in the above-unity regime and indicate feasible pathways toward $C \sim \mathcal{O}(1)$ or higher [65–67]. For the ^{87}Rb D-line, Ref. [68] further estimates $\Gamma \simeq 2\pi \times 6$ MHz and an effective cavity loss rate $\kappa \simeq 2\pi \times 0.06$ MHz in a motion-limited lattice configuration, while demonstrating that optimized atomic placement can in principle reach cooperativities as large as $C \gtrsim 10^4$.

Importantly, these constraints can be further relaxed by exploiting collective light–matter coupling in atomic ensembles [56, 66–70]. In the single-excitation manifold, symmetric collective states enhance the coupling as $\Omega_{\text{eff}} = \Omega\sqrt{N_{\text{atom}}}$ [71], thereby shortening the required evolution time and reducing the impact of dissipation. Using an experimentally motivated collective cooperativity benchmark $N_{\text{atom}}C \sim 10^8$ and taking the unitary-optimized value $\mathcal{F} \approx 0.97$ at $N = 100$ from Fig. 2(a), we estimate that post-selected preparation remains feasible with $\mathcal{F} \gtrsim 0.8$ while maintaining a high-success-probability operating regime. Together with the robustness to control errors discussed above, this suggests that deterministic high-fidelity preparation of photon-number states beyond $N = 100$ is within reach in state-of-the-art AMO cavity-QED platforms.

III. CONCLUSION

In this work, we introduced a multi-pulse JC–displacement protocol for scalable generation of large photon-number states. By alternating JC evolutions with phase-space displacements, the protocol engineers photon-number–dependent phases and converts them into selective interference in photon-number space, yielding high-fidelity preparation of photon-number states with $\mathcal{F} \gtrsim 0.95$ up to $N \simeq 200$ using shallow control depths. An optional qubit projection further removes residual qubit–field correlations with near-unity success probability. In addition, incorporating platform-specific constraints and dissipation into the optimization loop offers a practical pathway toward hardware-ready pulse sequences and further scaling to larger photon numbers.

Our results provide an experimentally accessible route to large- N photon-number state preparation using only native qubit–oscillator operations, applicable to cavity and circuit QED, trapped ions, and related AMO platforms [72, 73]. Looking forward, the same interference-engineering approach can be extended to prepare more general nonclassical bosonic resources, such as photon-number state superpositions and grid-like states [74], and to optimize probe states for quantum-enhanced sensing [75].

Note added. During the preparation of this manuscript, we became aware of a closely related preprint that introduces a similar photon-number space interference approach based on Kerr-induced nonlinear phase modulation for generating macroscopic photon-number states [76, 77].

ACKNOWLEDGEMENTS

This work was supported by the National Natural Science Foundation of China (No. 12304543), the Quantum Science and Technology - National Science and Technology Major Project (No. 2021ZD0302100), the Natural Science Foundation of Jiangsu Province (Nos. BK20250404 and BG2025017), the Youth Science and Technology Talent Support Program of Jiangsu Province (Nos. JSTJ-2024-507, JSTJ-2025-600 and JSTJ-2025-829), the Frontier Technology Research Program of Suzhou (No. SYG202322), and the Postgraduate Research & Practice Innovation Program of NUAU (No. xcxjh20252107).

Appendix A: Revivals and phase-space refocusing in the resonant JC model

Starting from $|\Psi_0\rangle = |e\rangle|\alpha\rangle$ with $|\alpha\rangle = e^{-|\alpha|^2/2} \sum_{n=0}^{\infty} \alpha^n/\sqrt{n!} |n\rangle$, the resonant Hamiltonian in Eq. (1) ($\omega_c = \omega_q$) produces the well-known collapse-and-revival dynamics of the cavity field [61, 78, 79]. At discrete revival times (indexed by ℓ), the field refocuses in phase space, as illustrated in Fig. 4.

Following the displacement $\hat{D}(\beta) = e^{\beta\hat{a}^\dagger - \beta^*\hat{a}}$, the qubit-

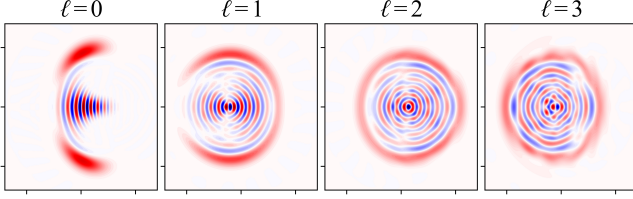


Figure 4. At discrete revival times (labeled by ℓ), the bosonic state refocuses in phase space and becomes Fock-like under the resonant Jaynes–Cummings Hamiltonian.

cavity state transforms into:

$$|\Psi(\beta, t)\rangle = \hat{D}(\beta)e^{-i\hat{H}t}|\Psi_0\rangle = \sum_{n=0}^{\infty} |K_n(t)\rangle \otimes |n\rangle \quad (\text{A1})$$

where $|K_m(t)\rangle$ represents the state of the atomic component. So the density matrix of the qubit-cavity state is:

$$\rho_{qc}(\beta, t) = \sum_{m=0}^{\infty} \sum_{m'=0}^{\infty} |K_m(t)\rangle \langle K_{m'}(t)| \otimes |m\rangle \langle m'|. \quad (\text{A2})$$

$|K_m\rangle$ describes the state of the qubit conditioned on the cavity field being in the photon-number state $|m\rangle$ after displacement by $D(\beta)$. By tracing out the qubit degrees of freedom, one obtains the reduced density operator for the cavity field:

$$\rho_c(\beta, t) \equiv \text{Tr}_q[\rho(\beta, t)] = \sum_{m=0}^{\infty} \sum_{n=0}^{\infty} P_{m,n}(\beta, t) |m\rangle \langle n|, \quad (\text{A3})$$

where $P_{m,n}$ denotes the coefficient of the matrix elements $|m\rangle \langle n|$. Therefore, the occupation probability of the photon-number state $|n\rangle$ is given by:

$$P_N(t) = \sum_{m,n=0}^{\infty} c_m c_n^* |\langle n | \hat{D}(\beta) | m \rangle|^2 (s_{m+1} s_{n+1} + \frac{\sqrt{mn}}{|\alpha|^2} s'_m s'_n), \quad (\text{A4})$$

where $s_m = \cos(\Omega\sqrt{m}t)$, $s'_m = \sin(\Omega\sqrt{m}t)$ and $c_m = \alpha^n e^{-|\alpha|^2/2} / \sqrt{n!}$.

The dominant contribution in this expression comes from terms where $m \approx n \approx |\alpha|^2$ ($m, n \gg 1$), as determined by both the high-frequency oscillating exponential factor and energy considerations. photon-number like states, particularly when $m \approx n \approx N$, are approximately realized at specific time instants given by

$$\Omega T_R^{(\ell)} \approx (2\ell + 1)\pi\sqrt{N}. \quad (\text{A5})$$

where $\ell \in \mathbb{N}$.

Appendix B: Rugged landscape and transfer initialization

At revival times, the qubit approaches an equatorial Bloch state, i.e., an equal-weight superposition of $|g\rangle$ and $|e\rangle$ with

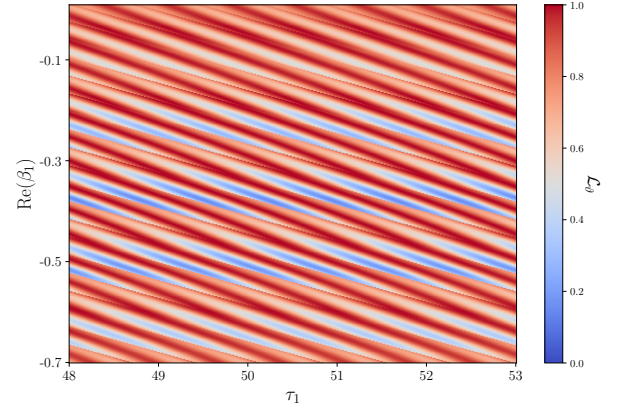


Figure 5. Non-convex loss landscape in a reduced subspace. Reduced loss \mathcal{L}_θ after a single JC segment followed by one displacement ($p = 1$), shown as a function of the interaction time τ_1 and the displacement quadrature $\text{Re}(\beta_1)$ (with $\text{Im}(\beta_1)$ fixed). The quasi-periodic stripe pattern reveals a dense set of competing local extrema, highlighting the intrinsic difficulty of the optimization even in this two-parameter slice.

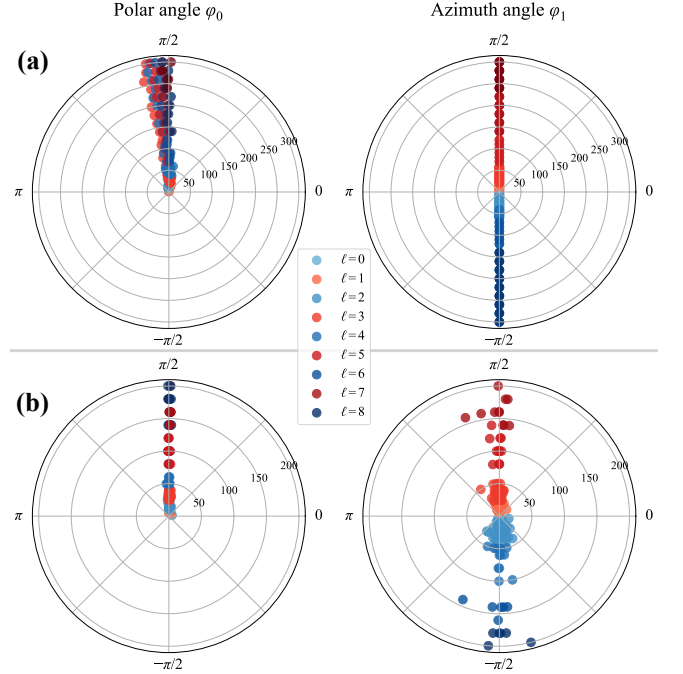


Figure 6. Distribution of optimal qubit projection angles. Optimized angles for the $p = 1$ seed (a) and the best- p protocol (b) [cf. Fig. 2(a)]. The optima correspond to Bloch vectors near the equator, consistent with the large- $|\alpha|$ JC half-revival “attractor”; for $\alpha = \sqrt{N} \in \mathbb{R}^+$ this yields $(\varphi_0, \varphi_1) \approx (\pi/2, \pm\pi/2)$ up to conventions.

$\langle \sigma_z \rangle \simeq 0$ [61, 80]. Starting from $|\Psi_0\rangle = |e\rangle |\alpha\rangle$ with $\alpha =$

\sqrt{N} , we write

$$|e\rangle = \frac{1}{\sqrt{2}}(|D_+(0)\rangle - |D_-(0)\rangle), \quad (\text{B1})$$

$$|D_{\pm}(0)\rangle = \frac{1}{\sqrt{2}}(|g\rangle \pm |e\rangle), \quad (\text{B2})$$

where $|D_{\pm}\rangle$ are eigenstates of the effective semiclassical Hamiltonian. In the large- N limit, the two branches evolve approximately independently, acquiring opposite dynamical phases,

$$|D_{\pm}(t)\rangle \approx \frac{1}{\sqrt{2}}(|g\rangle \pm e^{\mp i\Omega t/(2\sqrt{N})} |e\rangle). \quad (\text{B3})$$

At the revival instants $\Omega t = (2\ell + 1)\pi\sqrt{N}$, the phase factor $e^{\mp i\Omega t/(2\sqrt{N})} = e^{\mp i(2\ell + 1)\pi/2} = \mp i(-1)^{\ell}$, so the two branches converge to the same equatorial qubit state,

$$|D_+(t)\rangle \approx |D_-(t)\rangle \equiv \frac{1}{\sqrt{2}}(|g\rangle - i(-1)^{\ell} |e\rangle). \quad (\text{B4})$$

Thus qubit-cavity entanglement is strongly suppressed and the qubit is nearly pure, consistent with the optimized projection angles in Fig. 6.

Optimizing photon-number state preparation amounts to minimizing the loss \mathcal{L}_{ϑ} over $\vartheta = \{\tau, \beta, \varphi\}$. The landscape is highly non-convex even in low-dimensional slices: for $p = 1$ with fixed $\text{Im}(\beta_1)$, no projection, and target $N = 10$ ($\ell = 2$), the reduced loss \mathcal{L}_{ϑ} shows a dense, quasi-periodic multi-extremal structure over $\tau_1 \in [48, 53]$ and $\text{Re}(\beta_1) \in [-0.7, 0]$ (Fig. 5). This structure stems from interference between the two JC dynamical branches in Eq. (A4), readily trapping gradient-based or naive global searches.

These features motivate a transfer-initialized strategy based on the empirically and analytically established *parameter concentration* phenomenon, where near-optimal parameters cluster and can be transferred across related instances or circuit depths (e.g., the concentrated optimal projection angles in Fig. 6) [81, 82]. Accordingly, we adopt a transfer-initialized global-to-local optimizer, described next.

Appendix C: Hybrid optimization: GAdam with transfer initialization

We optimize the $3p + 2$ control parameters in Eq. (4) using a hybrid GAdam routine (Fig. 7), which combines global stochastic search with local Adam refinement to navigate the highly non-convex, multi-minima landscape.

Transfer initialization. As described in Step 1 of Fig. 7, the optimization is seeded by a transfer-initialization procedure based on an optimized single-layer ($p = 1$) solution at the same target photon-number N and revival index ℓ . The optimized parameters $\theta_1^{\text{opt}} = \{\tau_1^{\text{opt}}, \beta_1^{\text{opt}}, \varphi^{\text{opt}}\}$ define a physically meaningful global timing scale. This total evolution time, denoted T_{tar} , is fixed either to τ_1^{opt} or to the revival-based estimate $T_R^{(\ell)}$. Initial multi-pulse candidates are generated by randomly partitioning T_{tar} into p segments $\{\tau_k\}$ sub-

Algorithm 1 GAdam hybrid optimization

Input: Target photon number N ; revival index ℓ ; number of layers p ; loss function $\mathcal{L}(\theta)$; population size P ; elite size E ; number of generations G ; tournament size s ; crossover rate r_c ; mutation scale r_m ; Adam pre-optimization steps S_{pre} ; final Adam refinement steps S_{fin} ; minimum pulse duration τ_{min} ; displacement bound β_{max} ; time-mismatch tolerance ϵ_T .

Output: Optimized parameters $\theta^* = \{\tau^*, \beta^*, \varphi^*\}$.

1: Initialization from single-layer seed

Load optimized $p=1$ solution $\theta_1^{\text{opt}} = \{\tau_1^{\text{opt}}, \beta_1^{\text{opt}}, \varphi^{\text{opt}}\}$ for the same (N, ℓ) .

Set global target time $T_{\text{tar}} \leftarrow \tau_1^{\text{opt}}$ (or $T_R^{(\ell)}$ if specified).

for $i = 1, \dots, P$

$\varphi^{(i)} \leftarrow \varphi^{\text{opt}}, \beta_p^{(i)} \leftarrow \beta_1^{\text{opt}}$, and $\beta_k^{(i)} \leftarrow 0$ for $k = 1, \dots, p-1$.

Sample $\{\tau_k^{(i)}\}_{k=1}^p$ such that $\sum_{k=1}^p \tau_k^{(i)} = T_{\text{tar}}$ and $\tau_k^{(i)} \geq \tau_{\text{min}}$.

end for

2: Hybrid genetic and Adam

for $g = 1, \dots, G$

Adam pre-optimization

for $i = 1, \dots, P$

$\theta^{(i)} \leftarrow \text{Adam}(\theta^{(i)}, \mathcal{L}, S_{\text{pre}})$.

Enforce bounds: $\tau_k^{(i)} \geq \tau_{\text{min}}, |\beta_k^{(i)}| \leq \beta_{\text{max}}$.

end for

Compute fitness $f^{(i)} = 1 - \mathcal{L}(\theta^{(i)})$

Select elite set $\mathcal{P}_{\text{elite}}$ of top- E individuals.

Genetic reproduction

$\mathcal{P}_{\text{off}} \leftarrow \emptyset$

while $|\mathcal{P}_{\text{off}}| < P - E$

Select parents by tournament selection: $\theta^{(A)}, \theta^{(B)}$.

Apply uniform crossover with probability r_c .

Apply Gaussian mutation: $\theta^{\text{child}} \leftarrow \theta^{\text{child}} + \mathcal{N}(0, r_m^2)$.

Enforce bounds: $\tau_k \geq \tau_{\text{min}}, |\beta_k| \leq \beta_{\text{max}}$.

Soft time constraint: rescale $\tau_k \rightarrow \tau_k T_{\text{tar}} / \sum_j \tau_j$
if $|\sum_k \tau_k - T_{\text{tar}}| / T_{\text{tar}} > \epsilon_T$.

Add θ^{child} to \mathcal{P}_{off} .

end while

Update population: $\mathcal{P} \leftarrow \mathcal{P}_{\text{elite}} \cup \mathcal{P}_{\text{off}}$.

end for

$\theta^* \leftarrow \arg \min_{\theta \in \mathcal{P}} \mathcal{L}(\theta)$.

3: Adam refinement

$\theta^* \leftarrow \text{Adam}(\theta^*, \mathcal{L}, S_{\text{fin}})$. =0

Figure 7. GAdam optimization workflow.

ject to $\tau_k \geq \tau_{\text{min}}$, while inheriting the optimized final displacement β_p^{opt} and qubit measurement basis φ^{opt} . All intermediate displacements are initialized to zero. This construction places the initial population close to a physically relevant manifold, avoiding inefficient exploration of low-fidelity regions.

Hybrid genetic and Adam search. The optimization then proceeds iteratively over G generations (Step 2 of Fig. 7). Within each generation, every individual first undergoes a short Adam pre-optimization using the loss function $\mathcal{L}(\theta)$, which improves the overall population quality before genetic selection. After enforcing hard bounds on pulse durations and displacement amplitudes, the fitness of each individual is evaluated as $f = 1 - \mathcal{L}(\theta)$. An elite subset of the top- E individ-

uals is retained unchanged.

New candidates are generated through tournament-based parent selection, uniform crossover of control parameters, and Gaussian mutation. A soft global timing constraint is imposed: if the total duration deviates from T_{tar} beyond a relative tolerance ϵ_T , all τ_k are rescaled proportionally to restore the target total time. This allows the optimizer to freely redistribute pulse durations while preserving the global interference timescale set by the JC revival structure. The next gen-

eration is formed by combining the elite set with the newly generated offspring.

Final refinement. After G generations, the individual with the minimal loss is selected and subjected to a final, high-precision Adam refinement (Step 3 of Fig. 7). The resulting parameters $\theta^* = \{\tau^*, \beta^*, \varphi^*\}$ define the optimized composite-pulse sequence used in the performance and robustness analyses.

-
- [1] S. L. Braunstein and P. van Loock, Quantum information with continuous variables, *Rev. Mod. Phys.* **77**, 513 (2005).
- [2] J. Loredo, M. Broome, P. Hilaire, O. Gazzano, I. Sagnes, A. Lemaitre, M. Almeida, P. Senellart, and A. White, Boson sampling with single-photon fock states from a bright solid-state source, *Phys. Rev. Lett.* **118**, 130503 (2017).
- [3] H. Wang, Y. He, Y.-H. Li, Z.-E. Su, B. Li, H.-L. Huang, X. Ding, M.-C. Chen, C. Liu, J. Qin, *et al.*, High-efficiency multiphoton boson sampling, *Nature Photonics* **11**, 361 (2017).
- [4] F. Wolf, C. Shi, J. C. Heip, M. Gessner, L. Pezzè, A. Smerzi, M. Schulte, K. Hammerer, and P. O. Schmidt, Motional fock states for quantum-enhanced amplitude and phase measurements with trapped ions, *Nature Communications* **10**, 2929 (2019).
- [5] D. Gottesman, A. Kitaev, and J. Preskill, Encoding a qubit in an oscillator, *Phys. Rev. A* **64**, 012310 (2001).
- [6] M. Walschaers, Non-gaussian quantum states and where to find them, *PRX Quantum* **2**, 030204 (2021).
- [7] J. Deng, H. Dong, C. Zhang, Y. Wu, J. Yuan, X. Zhu, F. Jin, H. Li, Z. Wang, H. Cai, *et al.*, Observing the quantum topology of light, *Science* **378**, 966 (2022).
- [8] M. S. Winnel, J. J. Guanzon, D. Singh, and T. C. Ralph, Deterministic preparation of optical squeezed cat and gottesman-kitaev-preskill states, *Phys. Rev. Lett.* **132**, 230602 (2024).
- [9] A. L. Grimsmo and S. Puri, Quantum error correction with the gottesman-kitaev-preskill code, *PRX Quantum* **2**, 020101 (2021).
- [10] A. Blais, S. M. Girvin, and W. D. Oliver, Quantum information processing and quantum optics with circuit quantum electrodynamics, *Nat. Phys.* **16**, 247 (2020).
- [11] D. Hoshi, T. Nagase, S. Kwon, D. Iyama, T. Kamiya, S. Fujii, H. Mukai, S. Ahmed, A. F. Kockum, S. Watabe, *et al.*, Entangling schrödinger’s cat states by bridging discrete- and continuous-variable encoding, *Nature communications* **16**, 1309 (2025).
- [12] P. T. Grochowski and R. Filip, Optimal phase-insensitive force sensing with non-gaussian states, *Phys. Rev. Lett.* **135**, 230802 (2025).
- [13] T. J. Sturges, T. McDermott, A. Buraczewski, W. R. Clements, J. J. Renema, S. W. Nam, T. Gerrits, A. Lita, W. S. Kolthammer, A. Eckstein, I. A. Walmsley, and M. Stobińska, Quantum simulations with multiphoton fock states, *npj Quantum Information* **7**, 91 (2021).
- [14] C. Couteau, S. Barz, T. Durt, T. Gerrits, J. Huwer, R. Prevedel, J. Rarity, A. Shields, and G. Weihs, Applications of single photons in quantum metrology, biology and the foundations of quantum physics, *Nat. Rev. Phys.* **5**, 354 (2023).
- [15] M. Perarnau-Llobet, A. González-Tudela, and J. I. Cirac, Multimode fock states with large photon number: effective descriptions and applications in quantum metrology, *Quantum Science and Technology* **5**, 025003 (2020).
- [16] X. Deng, S. Li, Z.-J. Chen, Z. Ni, Y. Cai, J. Mai, L. Zhang, P. Zheng, H. Yu, C.-L. Zou, S. Liu, F. Yan, Y. Xu, and D. Yu, Quantum-enhanced metrology with large Fock states, *Nature Physics* [10.1038/s41567-024-02619-5](https://doi.org/10.1038/s41567-024-02619-5) (2024).
- [17] M. Fadel, N. Roux, and M. Gessner, Quantum metrology with a continuous-variable system, *Reports on Progress in Physics* **88**, 106001 (2025).
- [18] H.-S. Zhong, H. Wang, Y.-H. Deng, M.-C. Chen, L.-C. Peng, Y.-H. Luo, J. Qin, D. Wu, X. Ding, Y. Hu, *et al.*, Quantum computational advantage using photons, *Science* **370**, 1460 (2020).
- [19] L. S. Madsen, F. Laudenbach, M. F. Askarani, F. Rortais, T. Vincent, J. F. Bulmer, F. M. Miatto, L. Neuhaus, L. G. Helt, M. J. Collins, *et al.*, Quantum computational advantage with a programmable photonic processor, *Nature* **606**, 75 (2022).
- [20] A. D. O’Connell, M. Hofheinz, M. Ansmann, R. C. Bialczak, M. Lenander, E. Lucero, M. Neeley, D. Sank, H. Wang, M. Weides, *et al.*, Quantum ground state and single-phonon control of a mechanical resonator, *Nature* **464**, 697 (2010).
- [21] I. Aharonovich, D. Englund, and M. Toth, Solid-state single-photon emitters, *Nat. Photonics* **10**, 631 (2016).
- [22] S. P. Premaratne, F. Wellstood, and B. Palmer, Microwave photon fock state generation by stimulated raman adiabatic passage, *Nature Communications* **8**, 14148 (2017).
- [23] W. Wang, L. Hu, Y. Xu, K. Liu, Y. Ma, S.-B. Zheng, R. Vijay, Y. P. Song, L.-M. Duan, and L. Sun, Converting quasiclassical states into arbitrary fock state superpositions in a superconducting circuit, *Phys. Rev. Lett.* **118**, 223604 (2017).
- [24] A. Migdall, S. V. Polyakov, J. Fan, and J. C. Bienfang, *Single-photon generation and detection: physics and applications* (Academic Press, 2013).
- [25] R. Uppu, F. T. Pedersen, Y. Wang, C. T. Olesen, C. Papon, X. Zhou, L. Midolo, S. Scholz, A. D. Wieck, A. Ludwig, *et al.*, Scalable integrated single-photon source, *Sci. Adv.* **6**, eabc8268 (2020).
- [26] G. P. Teja, C. Kumar, L. c. v. Lachman, and R. Filip, Quantum non-gaussian high fock states of light pulses and their superpositions, *Phys. Rev. Res.* **7**, 033272 (2025).
- [27] Q. R. Rahman, I. Kladarić, M.-E. Kern, L. c. v. Lachman, Y. Chu, R. Filip, and M. Fadel, Genuine quantum non-gaussianity and metrological sensitivity of fock states prepared in a mechanical resonator, *Phys. Rev. Lett.* **134**, 180801 (2025).
- [28] M. Hofheinz, E. Weig, M. Ansmann, R. C. Bialczak, E. Lucero, M. Neeley, A. O’connell, H. Wang, J. M. Martinis, and A. Cleland, Generation of fock states in a superconducting quantum circuit, *Nature* **454**, 310 (2008).
- [29] H. Wang, M. Hofheinz, M. Ansmann, R. Bialczak, E. Lucero, M. Neeley, A. O’connell, D. Sank, J. Wenner, A. Cleland, *et al.*, Measurement of the decay of fock states in a superconducting quantum circuit, *Phys. Rev. Lett.* **101**, 240401 (2008).

- [30] M. Hofheinz, H. Wang, M. Ansmann, R. C. Bialczak, E. Lucero, M. Neeley, A. O'connell, D. Sank, J. Wenner, J. M. Martinis, *et al.*, Synthesizing arbitrary quantum states in a superconducting resonator, *Nature* **459**, 546 (2009).
- [31] P. Bertet, A. Auffeves, P. Maioli, S. Osnaghi, T. Meunier, M. Brune, J. M. Raimond, and S. Haroche, Direct measurement of the wigner function of a one-photon fock state in a cavity, *Phys. Rev. Lett.* **89**, 200402 (2002).
- [32] A. M. Brańczyk, T. Ralph, W. Helwig, and C. Silberhorn, Optimized generation of heralded fock states using parametric down-conversion, *New J. Phys.* **12**, 063001 (2010).
- [33] J. Tiedau, T. J. Bartley, G. Harder, A. E. Lita, S. W. Nam, T. Gerrits, and C. Silberhorn, Scalability of parametric down-conversion for generating higher-order fock states, *Phys. Rev. A* **100**, 041802 (2019).
- [34] X.-D. Zhou, S. Wang, H. Zhang, T.-B. Zhang, Y.-H. Chen, W. Qin, Y. Ning, and Y. Xia, Fast generation of 2n-photon fock states using shortcuts to adiabaticity and ultrastrong light-matter coupling, *Annalen der Physik* **535**, 2200348 (2023).
- [35] C. Sayrin, I. Dotsenko, X. Zhou, B. Peaudecerf, T. Rybarczyk, S. Gleyzes, P. Rouchon, M. Mirrahimi, H. Amini, M. Brune, *et al.*, Real-time quantum feedback prepares and stabilizes photon number states, *Nature* **477**, 73 (2011).
- [36] X. Zhou, I. Dotsenko, B. Peaudecerf, T. Rybarczyk, C. Sayrin, S. Gleyzes, J. Raimond, M. Brune, and S. Haroche, Field locked to a fock state by quantum feedback with single photon corrections, *Physical review letters* **108**, 243602 (2012).
- [37] B. Peaudecerf, C. Sayrin, X. Zhou, T. Rybarczyk, S. Gleyzes, I. Dotsenko, J. Raimond, M. Brune, and S. Haroche, Quantum feedback experiments stabilizing fock states of light in a cavity, *Phys. Rev. A* **87**, 042320 (2013).
- [38] M. Uria, P. Solano, and C. Hermann-Avigliano, Deterministic generation of large fock states, *Phys. Rev. Lett.* **125**, 093603 (2020).
- [39] V. Sivak, A. Eickbusch, H. Liu, B. Royer, I. Tsioutsios, and M. Devoret, Model-free quantum control with reinforcement learning, *Phys. Rev. X* **12**, 011059 (2022).
- [40] G. Teja and Chanchal, Distillation of optical fock states using atom-cavity systems, *Phys. Rev. Appl.* **20**, 044049 (2023).
- [41] C.-y. Zhang and J. Jing, Generating fock-state superpositions from coherent states by selective measurement, *Phys. Rev. A* **110**, 042421 (2024).
- [42] T. Fösel, S. Krastanov, F. Marquardt, and L. Jiang, Efficient cavity control with snap gates, arXiv preprint arXiv:2004.14256 (2020).
- [43] R. Yanagimoto, E. Ng, T. Onodera, and H. Mabuchi, Adiabatic fock-state-generation scheme using kerr nonlinearity, *Phys. Rev. A* **100**, 033822 (2019).
- [44] A. Lingenfelter, D. Roberts, and A. Clerk, Unconditional fock state generation using arbitrarily weak photonic nonlinearities, *Sci. Adv.* **7**, eabj1916 (2021).
- [45] N. Rivera, J. Sloan, Y. Salamin, J. D. Joannopoulos, and M. Soljačić, Creating large fock states and massively squeezed states in optics using systems with nonlinear bound states in the continuum, *PNAS* **120**, e2219208120 (2023).
- [46] X. Zhang, N. Wang, Z. Tian, Q. Liu, and Y. Gu, Deterministic generation of large fock states in coupled optical-optomechanical cavities, *Physical Review Research* **7**, 033158 (2025).
- [47] S. Li, Z. Ni, L. Zhang, Y. Cai, J. Mai, S. Wen, P. Zheng, X. Deng, S. Liu, Y. Xu, and D. Yu, Autonomous stabilization of fock states in an oscillator against multiphoton losses, *Phys. Rev. Lett.* **132**, 203602 (2024).
- [48] J. Fink, M. Göppl, M. Baur, R. Bianchetti, P. J. Leek, A. Blais, and A. Wallraff, Climbing the jaynes-cummings ladder and observing its nonlinearity in a cavity qed system, *Nature* **454**, 315 (2008).
- [49] M. M. Lund, F. Yang, V. R. Christiansen, D. Kornovan, and K. Mølmer, Subtraction and addition of propagating photons by two-level emitters, *Phys. Rev. Lett.* **133**, 103601 (2024).
- [50] A. Pasharavesh and M. Bajcsy, Multi-photon fock state generation via selective single photon subtraction in a cascaded waveguide qed system, *Advanced Quantum Technologies* , 2400616 (2025).
- [51] R. W. Heeres, B. Vlastakis, E. Holland, S. Krastanov, V. V. Albert, L. Frunzio, L. Jiang, and R. J. Schoelkopf, Cavity state manipulation using photon-number selective phase gates, *Phys. Rev. Lett.* **115**, 137002 (2015).
- [52] A. Eickbusch, V. Sivak, A. Z. Ding, S. S. Elder, S. R. Jha, J. Venkatraman, B. Royer, S. M. Girvin, R. J. Schoelkopf, and M. H. Devoret, Fast universal control of an oscillator with weak dispersive coupling to a qubit, *Nat. Phys.* **18**, 1464 (2022).
- [53] J. Landgraf, C. Flühmann, T. Fösel, F. Marquardt, and R. J. Schoelkopf, Fast quantum control of cavities using an improved protocol without coherent errors, *Phys. Rev. Lett.* **133**, 260802 (2024).
- [54] A. Muñoz de las Heras, C. Tabares, J. T. Schneider, L. Tagliacozzo, D. Porras, and A. González-Tudela, Photonic quantum metrology with variational quantum optical nonlinearities, *Phys. Rev. Res.* **6**, 013299 (2024).
- [55] A. M. de las Heras, D. Porras, and A. González-Tudela, Improving quantum metrology protocols with programmable photonic circuits, *Nanophotonics* **14**, 2075 (2025).
- [56] F. Mivehvar, F. Piazza, T. Donner, and H. Ritsch, Cavity qed with quantum gases: New paradigms in many-body physics, *Advances in Physics* **70**, 1 (2021).
- [57] A. Blais, A. L. Grimsmo, S. M. Girvin, and A. Wallraff, Circuit quantum electrodynamics, *Rev. Mod. Phys.* **93**, 025005 (2021).
- [58] Y. Wu and X. Yang, Jaynes-cummings model for a trapped ion in any position of a standing wave, *Physical review letters* **78**, 3086 (1997).
- [59] D. Leibfried, R. Blatt, C. Monroe, and D. Wineland, Quantum dynamics of single trapped ions, *Reviews of Modern Physics* **75**, 281 (2003).
- [60] J. Ye and P. Zoller, Essay: Quantum sensing with atomic, molecular, and optical platforms for fundamental physics, *Phys. Rev. Lett.* **132**, 190001 (2024).
- [61] J. Gea-Banacloche, Collapse and revival of the state vector in the jaynes-cummings model: An example of state preparation by a quantum apparatus, *Physical Review Letters* **65**, 3385 (1990).
- [62] R. Robinett, Quantum wave packet revivals, *Physics Reports* **392**, 1 (2004).
- [63] L. Sun, A. Petrenko, Z. Leghtas, B. Vlastakis, G. Kirchmair, K. Sliwa, A. Narla, M. Hatridge, S. Shankar, J. Blumoff, *et al.*, Tracking photon jumps with repeated quantum non-demolition parity measurements, *Nature* **511**, 444 (2014).
- [64] L. D. Burkhardt, J. D. Teoh, Y. Zhang, C. J. Axline, L. Frunzio, M. Devoret, L. Jiang, S. Girvin, and R. Schoelkopf, Error-detected state transfer and entanglement in a superconducting quantum network, *PRX Quantum* **2**, 030321 (2021).
- [65] Z. Yan, J. Ho, Y.-H. Lu, S. J. Masson, A. Asenjo-Garcia, and D. M. Stamper-Kurn, Superradiant and subradiant cavity scattering by atom arrays, *Phys. Rev. Lett.* **131**, 253603 (2023).
- [66] Y. Liu, Z. Wang, P. Yang, Q. Wang, Q. Fan, S. Guan, G. Li, P. Zhang, and T. Zhang, Realization of strong coupling between deterministic single-atom arrays and a high-finesse miniature

- optical cavity, *Phys. Rev. Lett.* **130**, 173601 (2023).
- [67] A. L. Shaw, A. Soper, D. Shadmany, A. Kumar, L. Palm, D.-Y. Koh, V. Kaxiras, L. Taneja, M. Jaffe, D. I. Schuster, *et al.*, A cavity-array microscope for parallel single-atom interfacing, *Nature* **650**, 320 (2026).
- [68] D. Castells-Graells, J. I. Cirac, and D. S. Wild, Cavity quantum electrodynamics with atom arrays in free space, *Phys. Rev. A* **111**, 053712 (2025).
- [69] R. Pennetta, D. Lechner, M. Blaha, A. Rauschenbeutel, P. Schneeweiss, and J. Volz, Observation of coherent coupling between super- and subradiant states of an ensemble of cold atoms collectively coupled to a single propagating optical mode, *Phys. Rev. Lett.* **128**, 203601 (2022).
- [70] M. Blaha, A. Johnson, A. Rauschenbeutel, and J. Volz, Beyond the tavis-cummings model: Revisiting cavity qed with ensembles of quantum emitters, *Phys. Rev. A* **105**, 013719 (2022).
- [71] M. Fleischhauer and M. D. Lukin, Quantum memory for photons: Dark-state polaritons, *Phys. Rev. A* **65**, 022314 (2002).
- [72] F. Haas, J. Volz, R. Gehr, J. Reichel, and J. Estève, Entangled states of more than 40 atoms in an optical fiber cavity, *Science* **344**, 180 (2014).
- [73] V. Srivastava, S. Jandura, G. K. Brennen, and G. Pupillo, Entanglement-enhanced quantum sensing via optimal global control with neutral atoms in a cavity, *Phys. Rev. Lett.* **136**, 060806 (2026).
- [74] B. L. Brock, S. Singh, A. Eickbusch, V. V. Sivak, A. Z. Ding, L. Frunzio, S. M. Girvin, and M. H. Devoret, Quantum error correction of qudits beyond break-even, *Nature* **641**, 612 (2025).
- [75] C. H. Valahu, M. P. Stafford, Z. Huang, V. G. Matsos, M. J. Millican, T. Chalermputisarak, N. C. Menicucci, J. Combes, B. Q. Baragiola, and T. R. Tan, Quantum-enhanced multiparameter sensing in a single mode, *Science Advances* **11**, eadw9757 (2025).
- [76] M. Li, W. Cai, Z. Hua, Y. Xu, Y. Zhou, Z.-J. Chen, X.-B. Zou, G.-C. Guo, L. Sun, and C.-L. Zou, Scalable generation of macroscopic fock states exceeding 10,000 photons, *arXiv preprint arXiv:2601.05118* (2026).
- [77] Y. Xu, Y. Zhou, Z. Hua, L. Sun, J. Zhou, W. Wang, W. Cai, H. Huang, L. Xiao, G. Xue, H. Yu, M. Li, C.-L. Zou, and L. Sun, Principles of optics in the fock space: Scalable manipulation of giant quantum states (2026), *arXiv:2601.10325 [quant-ph]*.
- [78] J. H. Eberly, N. B. Narozhny, and J. J. Sánchez-Mondragón, Periodic spontaneous collapse and revival in a simple quantum model, *Phys. Rev. Lett.* **44**, 1323 (1980).
- [79] H.-I. Yoo and J. Eberly, Dynamical theory of an atom with two or three levels interacting with quantized cavity fields, *Physics Reports* **118**, 239 (1985).
- [80] J. Gea-Banacloche, Atom- and field-state evolution in the jaynes-cummings model for large initial fields, *Phys. Rev. A* **44**, 5913 (1991).
- [81] V. Akshay, D. Rabinovich, E. Campos, and J. Biamonte, Parameter concentrations in quantum approximate optimization, *Phys. Rev. A* **104**, L010401 (2021).
- [82] L. Zhou, S. Wang, S. Choi, H. Pichler, and M. D. Lukin, Quantum approximate optimization algorithm: Performance, mechanism, and implementation on near-term devices, *Phys. Rev. X* **10**, 021067 (2020).